Science Bulletin 64 (2019) 650–652

Contents lists available at ScienceDirect

Science Bulletin

journal homepage: www.elsevier.com/locate/scib

Short Communication

Complex multiple-segment ruptures of the 28 September 2018, Sulawesi, Indonesia, earthquake

Yong Zhang [a,*], Yun-Tai Chen [a,b], Wanpeng Feng [c]

[a] School of Earth and Space Sciences, Peking University, Beijing 100871, China
[b] Institute of Geophysics, China Earthquake Administration, Beijing 100081, China
[c] Guangdong Provincial Key Laboratory of Geodynamics and Geohazards, School of Earth Sciences and Engineering, Sun Yat-sen University, Guangzhou 510275, China

ARTICLE INFO

Article history:
Received 24 December 2018
Received in revised form 1 April 2019
Accepted 2 April 2019
Available online 12 April 2019

On 28 September 2018, an M_W7.5 earthquake struck Palu, Indonesia, and caused a large number of deaths and economic losses. Seismic moment tensor solutions determined by different institutes consistently suggest that this earthquake is overall a strike-slip event. However, it caused an unexpected large-scale tsunami around the Palu bay area. Commonly, the displacements of hanging wall and foot wall of a strike-slip event are mainly in horizontal directions, and are considerably weak in vertical components. Since vertical deformations are critical for tsunami generations, it is necessary to identify whether the tsunami is related to the source process or not. For this purpose, investigations of the source process are needed [1].

We first estimate the seismic moment tensor solution by using P waves of 24 teleseismic stations with the epicentral distances ranging from 30° to 90° (Fig. S1 online). The Green's functions were calculated based on the CRUST2.0 crust model [2] and the AK135 mantle model [3] by using the codes of Wang et al. [4]. Only P waves on vertical components were considered and band pass filtered with 0.01–0.02 Hz. Following the practice of Zhang et al. [5], the inversion consists of two steps, i.e., first solving the moment tensor (MT) with triangle source time function (STF), and then solving the MT and complex-shaped STF iteratively. The final results are shown in Fig. S2 (online). The seismic scalar moment is 2.1×10^{20} Nm (about M_W7.5). The strike/dip/rake of the two nodal planes are 352°/64°/−11° and 87°/80°/−154°, respectively. Based on the aftershock distribution and the local tectonic background around the epicentral region, the north–south extending plane (352°/64°/−11°) was supposed as the causative fault.

The source information of rupture direction can be demonstrated by the azimuth-dependent apparent source time function (ASTF). With the obtained moment tensor solution, we retrieved the ASTFs at the 24 teleseismic stations (Fig. S1 online). The Doppler Effects of the rupture propagations are clearly indicated by ASTFs. From Fig. 1, the ratios between the peak moment rate and the scalar moment of these ASTFs show significant azimuth variations: they are largest to the south of the epicenter, suggesting the rupture mainly propagated to the south.

We used an ALOS-2 L-band interferometric pair of 20180927 and 20181011 to retrieve the co-seismic displacements along the satellite flight. The two scenes of ALOS-2 data are in track 25 in the descending orbit with a heading angle of 192 clockwise from the north. An InSAR automated processing environment, gInSAR [6] was applied to conduct the InSAR processing and a 30-m-resolution SRTM data was used in the processing. The processed co-seismic InSAR deformation is shown in Fig. 1a. Most deformation occurred to the south of the epicenter, well consistent with the southward extension of ruptures indicated by ASTF analysis. Based on the deformation data, we constructed a 6-segment fault model with each of different strikes (Fig. 1a). Since there is no information available for the dip angle, a uniform dip of 64°, which is determined from the seismic moment tensor inversion, was assumed for all 6 segments.

With the constructed fault model, we jointly inverted the teleseismic, regional seismic, and InSAR data to estimate the rupture process by using the technique of Zhang et al. [7]. In the inversion, we assume a maximum rupture velocity (V_r^{max}) of 6 km/s, and a maximum sub-fault rupture duration of 30 s. This means that for a given sub-fault d kilometers away from the hypocenter, the rupture velocity can range from $d/(d/6+30)$ km/s to 6 km/s. The relatively fast rupture velocity assumed for the earthquake is because that rupture velocity of strike-slip events are prone to be fast, especially for those breaking through the ground surface [8]. In the joint inversion, the teleseismic, regional and the geodetic

* Corresponding author.
E-mail address: zhang-yong@pku.edu.cn (Y. Zhang).

https://doi.org/10.1016/j.scib.2019.04.018
2095-9273/

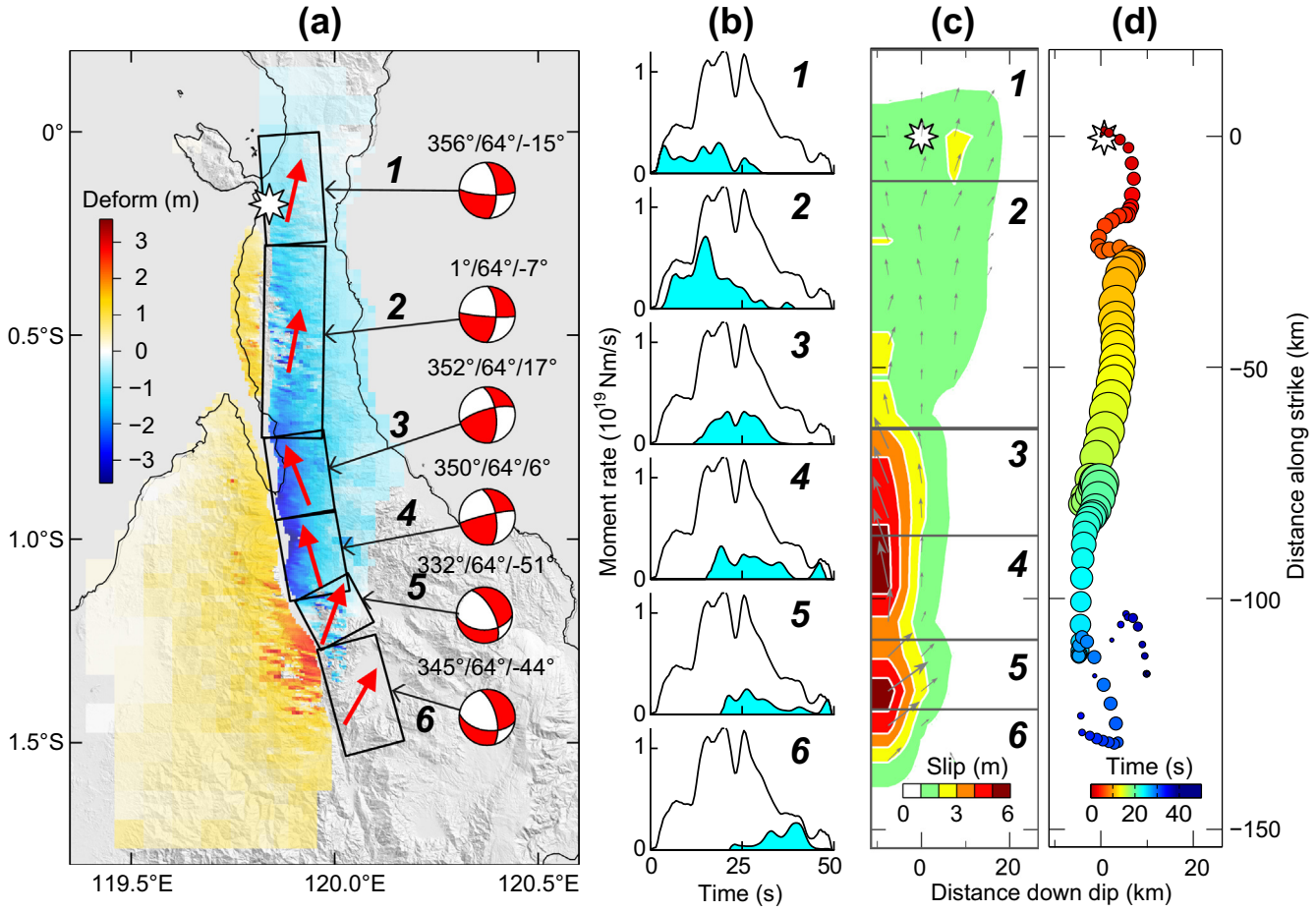

Fig. 1. Surface deformation, fault and rupture models. (a) Colors present the InSAR surface deformations. Rectangles are the surface projections of 6 fault segments. Red arrows and beach balls denote the movement directions of the hanging walls and average mechanisms of each segment. (b) Source times functions (cyan areas) of the 6 fault segments. The source time function plotted with black line is the earthquake source time function, i.e., the summation of those of all segments. (c) Fault slip distribution. (d) The temporal evolution of locations of centroid moment.

deformation data were equally weighted. We have also tried other weights, and found rupture model does not change significantly if the weight variations are less than one order of magnitude. Since the epicenter is located around the fault trace, we assumed the rupture initiated at a depth of 10 km and close to hypocenter.

The source time functions and fault slip distributions of each fault segment obtained from the joint inversion are depicted in Fig. 1b,c. The length of the ruptured fault is about 140 km. The slips extended to a deeper depth in the north (segments 1–2), but mainly concentrated at shallow depth in the south (segments 3–6). The peak slip is 2–3 m on segments 1–2 in the north, significantly less than 5–6 m on segments 3–6 in the south. Because of the relatively broader slip area and the weak slip amplitude, the average stresses drop is about 4 MPa in the north, less than that of 10 MPa in the south. In addition, the rakes also vary along the strike. Pure strike-slips were found on segments 1–4 in the north, while on segments 5–6 in the south, the normal-faulting components are even comparable with the strike-slips.

The source duration is about 50 s. Considering the fault length of 140 km, the average rupture velocity is about 2.8 km/s. However, the rupture did not continuously propagate to the south with a constant velocity [9]. From the spatial–temporal variations of the fault slip rate (Fig. S3 online), several rupture stages can be distinguished. The first stage is 0–12 s. In this period ruptures propagated to the south unilaterally with a rupture velocity of about 2.0 km/s. In 12–18 s, the ruptures extended along the

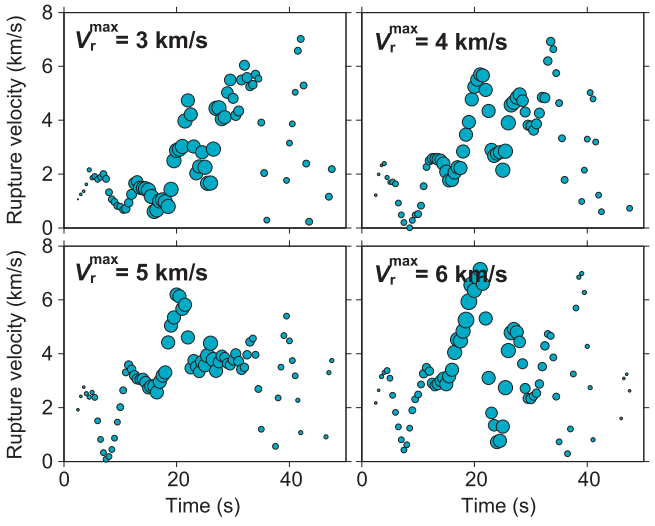

Fig. 2. Propagation velocity of moment centroid obtained with different maximum rupture velocity (V_r^{max}).

down-dip direction and formed a broad slip area. In 18–40 s, ruptures continued propagating southward with an average velocity of about 3.9 km/s. If considering the temporal variation of the moment centroid, the rupture velocity show very high values at

two time periods, i.e., 5.9 km/s in 14.5–23 s and 4.9 km/s at 26–33.5 s (Fig. S4 online), which have exceeded the shear velocity around the slip area. Synthetics of the rupture model well fit both the waveform and deformation data (Figs. S5–S7 online).

To check if the supershear ruptures depend on the maximum rupture velocity (V_r^{max}) assumed in the inversion, we tested several other values of V_r^{max} (3, 4 and 5 km/s), and compared the propagation velocities of moment centroid with that obtained with V_r^{max} = 6 km/s (Fig. 2). It indicates that even with a relatively small value of V_r^{max} (3 km/s), the transient rupture velocity is likely to be fast. The four models shown in Fig. 2 consistently suggest that the rupture propagated slowly in 0–10 s, and then accelerated to at least 4 km/s at about 20 s. The fast ruptures are coincident with other results of back projection [9]. In our model, however, rupture accelerated in the first 10 s, rather than propagated with a constant speed [9].

The 28 September 2018 M_W7.5 Sulawesi earthquake suggests complex fault geometry and rupture history. From co-seismic InSAR deformation data, it is clear that multiple segments were ruptured during the earthquake. Maybe because of the complexity in fault geometry, the rupture shows variable velocity during its southward propagation. Accordingly, the slip also show heterogeneities along both strike and down-dip directions. In addition, different to the strike-slip mechanism in the north, significant normal-faulting component appears at the south end of the ruptured fault. For this case, it suggests that not only the fault geometric complexity [10–12], but also the rake changes may play important roles in termination of the earthquake ruptures.

However, the normal-faulting components are mainly located on land, which should not be the major cause of the tsunami disasters. Since only a small part of fault strike-slip area (around the border between segments 2 and 3) is beneath the seafloor, it is far from enough to generate significant vertical seafloor deformations. It is possible that some other fault segments beneath the seafloor, which cannot be distinguished by seismic and deformation data and were not considered in this work, may have ruptured and generated the tsunami. Other factors, such as submarine landslides, which could be triggered by strong ground motions of the super-shear ruptures, can also result in the tsunami disasters.

Conflict of interest

The authors declare that they have no conflict of interest.

Acknowledgments

This work was supported by the National Natural Science Foundation of China (41822401 and 41574035).

Author contributions

Yong Zhang performed the inversion and drafted the manuscript. Yun-Tai Chen provided helpful suggestions and revised the manuscript. Wanpeng Feng processed the InSAR data.

Appendix A. Supplementary data

Supplementary data to this article can be found online at https://doi.org/10.1016/j.scib.2019.04.018.

References

[1] Chen Y, Hu J, Peng F. Seismological challenges in earthquake hazards reduction-Reflections on the 2008 Wenchuan earthquake. Sci Bull 2018;63:1159–66.
[2] Bassin C. The current limits of resolution for surface wave tomography in North America. Eos Trans AGU 2000:81.
[3] Kennett BLN, Engdahl ER, Buland R. Constraints on seismic velocities in the earth from traveltimes. Geophys J Int 1995;122:108–24.
[4] Wang R, Heimann S, Zhang Y, et al. Complete synthetic seismograms based on a spherical self-gravitating Earth model with an atmosphere-ocean-mantle-core structure. Geophys J Int 2017;210:1739–64.
[5] Zhang Y, Chen YT, Song J. Source mechanism and rupture characteristics of the 2018 M_W4.3 Yongqing earthquake. Chin Sci Bull 2018;63:2296–301 (in Chinese).
[6] Feng W, Omari K, Samsonov S. An automated insar processing system: potentials and challenges, 2016 IEEE International Geoscience and Remote Sensing Symposium (IGARSS). 2016, https://doi.org/10.1109/IGARSS.2016.7729830.
[7] Zhang Y, Feng W, Chen YT, et al. The 2009 L'Aquila M_W 6.3 earthquake: a new technique to locate the hypocentre in the joint inversion of earthquake rupture process. Geophys J Int 2012;191:1417–26.
[8] Xu J, Zhang H, Chen X. Rupture phase diagrams for a planar fault in 3-D full-space and half-space. Geophys J Int 2015;202:2194–206.
[9] Bao H, Ampuero J, Meng L, et al. Early and persistent supershear rupture of the 2018 magnitude 7.5 Palu earthquake. Nat Geosci 2019. https://doi.org/10.1038/s41561-018-0297-z.
[10] King G, Nabelek J. Role of fault bends in the initiation and termination of earthquake rupture. Science 1985;228:984–8.
[11] Zhang P, Slemmons D, Mao F. Geometric pattern, rupture termination and fault segmentation of the Dixie Valley—Pleasant Valley active normal fault system, Nevada, USA. J Struct Geol 1991;13:165–76.
[12] Zhang Y, Wang R, Walter TR, et al. Significant lateral dip changes may have limited the scale of the 2015 M_W 7.8 Gorkha earthquake. Geophys Res Lett 2017;44:8847–56.

Yong Zhang is currently an assistant professor in Peking University. He got his Ph.D. degree from Peking University in 2008, and then worked at Institute of Geophysics, China Earthquake Administration from 2008 to 2014. He mainly engages in earthquake source inversion, aiming to explore the complexities in rupture process and fault geometry, and to provide timely source information to emergency responses of significant earthquakes.